2000: The Journal of Astronomical Data 6, 2.

Radio spectroscopy of long-term 22 GHz observations of water maser outbursts in W49 N*

T. Liljeström

Metsähovi Radio Observatory, Helsinki University of Technology,
Otakaari 5.A, FIN-02150 Espoo, Finland (Tarja.Liljestrom@hut.fi)

Received 27 July 1999; accepted 29 November 1999

Abstract

High signal-to-noise spectroscopic results are presented for the powerful water maser cluster W49 N, obtained with the Metsähovi radio telescope from a 2.5 year long monitoring period. Gaussian line parameters of 108 maser outburst features as function of time are presented (108 electronic tables in ASCII format). These contain in total some 1740 Gaussian fits of the masing water line at 22 GHz. The flux density curves of 168 maser outbursts have been ordered as function of time and are displayed in 11 electronically available figures. Correlated outburst events are briefly discussed.

Key Words:ISM: individual (W49 N)—masers—shock waves—turbulence—radio lines: interstellar—astronomical data bases: miscellaneous

1 Introduction

Water masers trace warm molecular gas behind shock waves driven mainly by energetic jets and winds from very young stellar objects (Genzel et al. 1977; Walker et al. 1982; Gwinn et al. 1992; Gwinn 1994a, 1994b; Greenhill et al. 1998). Besides these outflow shocks, infalling protostellar envelopes or expanding compact HII regions may shock dense gas and produce water masers (e.g., Genzel et al. 1981; Leppänen et al. 1998). Because W49 N is the most luminous and rich water maser cluster in our Galaxy, it is an ideal laboratory to study shocks and turbulence. Single-antenna monitoring programmes of W49 N at 22 GHz have been reported by Sullivan (1971, 1973), Gammon (1976), Genzel and Downes (1977), Little et al. (1977), White and Macdonald (1979) and Liljeström et al. (1989).

The long-term W49 N observations of Liljeström et al. (1989) were carried out during the same time period and with the same velocity resolution as the 5-epoch VLBI observations of this source (Gwinn et al. 1992; Gwinn 1994a, Gwinn 1994b). Combining these two water maser databases, Liljeström and Gwinn (1999) were able to observationally fix the free

*Preliminary reductions done 1983 at Helsinki University Observatory model parameters in the comprehensive shock and maser models of Hollenbach and McKee (1979, 1989) and Elitzur et al. (1989). This enabled a detailed analysis of the postshocked conditions in W49 N and resulted to a straightforward determination of some 20 shock and maser parameters of this source (Liljeström and Gwinn 1999).

This paper presents and analyses the Gaussian line parameters of the water maser spectra reported by Liljeström et al. (1989). Section 2 summarizes the observations. Sections 3.1 and 3.2 consider the data and their uncertainties. Correlated outburst events are briefly discussed in Section 3.3.

2 Observations

The basic observations of the present study have been reported by Liljeström et al. (1989) in form of a spectral atlas of 22 GHz spectra in the velocity range -330 to 220 $\mathrm{km\,s^{-1}}$. The observations were carried out with the 13.7-m Metsähovi radio telescope[1] in position switching mode. At 22.2 GHz the half-power beam width of the antenna is $4.0'$. The receiver frontend was a room temperature Schottky-barrier mixer and the backend a narrowband (11.1 MHz) acousto-optical spectrometer with a channel width of 10.8 kHz and a frequency resolution of 20 kHz (corresponding to a velocity resolution of 0.27 $\mathrm{km\,s^{-1}}$ at 22.2 GHz). A good frequency stability (to within ± 0.005 of the frequency resolution) was achieved through a servo control of the zero point (Malkamäki 1983). The Doppler velocities of the maser features refer to the Local Standard of Rest (lsr) and are given with respect to the weighted mean frequency (22.235080 GHz) of the six hyperfine components of the masing 6_{16} - 5_{23} rotational transition of the H_2O molecule. During the 2.5 year monitoring period (December 1980 - June 1983) the observations were done at an average time interval of one week.

Because the high-resolution spectrometer covered only a bandwidth of 11.1 MHz, W49 N was observed in four scans centred at different velocities with a good overlap of the four velocity regions (see Liljeström et al. 1989). The spectra were calibrated with the well-known chopper-wheel calibration technique (Ulich and Haas 1976), which provided the correction for atmospheric attenuation. The pointing was checked with cross scans through the continuum sources 3C 84 and 3C 286. The conversion factor of the measured antenna temperature to flux density was 23 Jy/K for a point source. This conversion factor takes the attenuation factor (0.8) of the radome properly into account. The conversion factor has been checked with standard 22 GHz continuum sources using the broadband spectrometer (bandwidth 100 MHz; channel width 0.79 $\mathrm{km\,s^{-1}}$). The comparison of the Jansky scales of the broadband and narrowband spectrometers was based on the requirement of equal integrated flux densities in both spectrometers in the central velocity range of -15 to 30 $\mathrm{km\,s^{-1}}$. Systematic fluctuations in the flux density, caused by weather (e.g., wet snow on the radome) and/or gain problems, were estimated to affect the relative accuracy less than 10%.

The average rms noise in the flux density of the spectra was 30 Jy. Because masers inside (outside) the Doppler velocity range of the dense ambient medium, $-2 < v_{lsr} < 18$ $\mathrm{km\,s^{-1}}$ (Serabyn et al. 1993), have different properties (Liljeström and Gwinn 1999), the masers within (outside) this velocity range are referred to as "inside" ("outside") masers. At outburst maximum of the median inside (outside) maser, the signal-to-noise ratio is 675 (75). In the whole data the signal-to-noise ratio of the weakest and strongest outburst maser line is 7.2 and 2490, respectively.

[1] Operated by Metsähovi Radio Observatory, Helsinki University of Technology.

3 Results and discussion

3.1 The data

Water maser features commonly show dramatic variations in flux density as function of time. Usually, the flux density of a maser feature remains constant for long periods, then increases rapidly, remains at high level for a time, and then returns to about the original level. These short-lived, dramatic increases in flux density are termed as "outbursts". The durations of the observed outbursts lasted from 9 to 305 days. From the 2.5 year long monitoring period of W49 N, some 168 water maser outbursts were found, of which 146 were reasonably well covered during the outbursts. Because one and the same maser feature may show recurring outbursts, the number of maser outburst features is reduced to 108. The 168 outbursts have been ordered as function of time and displayed in Figures 1 a-k (electronically available as the files w49nfig1a.ps, w49nfig1b.ps, etc). As an example, Figure 1 shows the file w49nfig1g.ps. The velocity labels in these figures refer exceptionally to the rest frequency, 22.23512 GHz, of the hyperfine component F = 5 - 4. All velocities given in the labels of Figures 1 a-k will be smaller by 0.54 km s^{-1}, if the weighted mean frequency of the six hyperfine components is used (the standard practice).

All maser spectra of the outbursts were documented by fitting Gaussian profiles vs. velocity to the observed spectra. Before each Gaussian fit a first order baseline (determined far away from the crowded region of maser features) was removed from the spectrum. The Gaussian fits were performed with the POPS (People-Oriented Parsing Service) spectral line analysis package of the National Radio Astronomy Observatory (NRAO), USA. The routine fits a Gaussian function over a specified interval of the scan of the form $F = F_0\ exp[-4\ \ln 2\ (v - v_0)^2/(\Delta v)^2]$, where F is the flux density, Δv the full width at half maximum (FWHM) of the line profile, and the subscript zero refers to the peak value of the line. The routine requires initial values of the line centre, half-width (in channels) and height (in Kelvins). Then the routine iterates the height, centre location and half-width of the Gaussian until a satisfactory fit is obtained.

The Gaussian fits provided the peak flux density, the line velocity, and the linewidth of each of the 108 outburst features as function of time. The Gaussian results are presented in 108 electronic tables (in ASCII format), named systematically w49nxxxx.x.txt, where xxxx.x is the line velocity of the outburst feature as listed in Table 1. The data files contain the following information.

Column 1: The Julian date subtracted by 2440000 days.
Column 2: The Doppler velocity, v_{lsr}, of the line (in units of km s^{-1}), obtained from a Gaussian fit to the line profile.
Column 3: The statistical error in line velocity (absolute value in units of km s^{-1}).
Column 4: The linewidth (FWHM), in units of km s^{-1}, obtained from a Gaussian fit to the line profile. The linewidths have been corrected for the velocity resolution of the spectrometer.
Column 5: The statistical error in linewidth (absolute value in units of km s^{-1}).
Column 6: The flux density of the line peak (in Jy units), obtained from a Gaussian fit to the line profile.
Column 7: The statistical error in flux density (absolute value in units of km s^{-1}).
Column 8: The rms noise (in Jy units).

Three examples of the 108 data files are given in Tables 2 - 4, which are graphically displayed in Figures 2 - 4.

Sometimes the tables may show a few missing values in the line velocity and half-width. This indicates that at the observing epoch the outburst feature was either too weak for a successful Gaussian fit, or that it was blended with an adjacent maser feature, which was spaced too closely in Doppler velocity and therefore caused a failure in the Gaussian fitting procedure. In these cases both line velocity and half-width are missing in the tables. However, if the Gaussian fit was successful after fixing, e.g., the line velocity, only this fixed line velocity was removed. Generally, in order to resolve two adjacent maser features, at least one velocity channel (width 0.135 $\mathrm{km\,s^{-1}}$) between the line peaks is needed (the flux density in this channel should be below the half-value of the flux density of the line peaks in the adjacent channels). Thus, the velocity separation between two adjacent maser line peaks must be at least 0.27 $\mathrm{km\,s^{-1}}$.

3.2 Uncertainties

During maser outbursts blends of adjacent maser features may cause more complex line profiles, especially at start or end of outbursts. However, close to outburst maximum, the line shape is usually well matched with a Gaussian profile. In the error analysis of the Gaussian fits the rms noise in the observed spectra plays a central role. The average rms noise of inside masers (37 Jy) is somewhat higher than for outside masers (29 Jy). This is due to the shorter integration times used for the stronger maser features in the central low-velocity region of W49 N.

The statistical error in flux density of the line peak is estimated as the mean error of the flux density fluctuations over the half-width considered, $dF = \sigma/n^{0.5}$, where σ is the rms noise and n the number of the channels covered by the half-width of the line. For the median inside maser (F = 21500 Jy), the error in flux density ($\pm$13 Jy) produces a relative error of 0.06%. For the median outside maser (F = 1365 Jy), the error, $dF = \pm 11$ Jy, yields a relative error of 0.8%.

The error in linewidth, $d(\Delta v)$, is estimated from $(dF/F)\times\Delta v$. The median linewidths, 1.26 $\mathrm{km\,s^{-1}}$ (inside masers) and 1.10 $\mathrm{km\,s^{-1}}$ (outside masers), have an uncertainty of $\pm$0.00076 $\mathrm{km\,s^{-1}}$ and $\pm$0.0088 $\mathrm{km\,s^{-1}}$, respectively.

The error in the Doppler velocity of the line, dv_{lsr}, is estimated from $d(\Delta v)/2$, which yields $\pm$0.00038 $\mathrm{km\,s^{-1}}$ and $\pm$0.0044 $\mathrm{km\,s^{-1}}$ for the median inside and outside maser, respectively. This corresponds to 0.14% (median inside maser) and 1.6% (median outside maser) of the velocity resolution of the spectrometer (0.27 $\mathrm{km\,s^{-1}}$).

Even for the weakest outburst in the whole database, 133 Jy, the statistical errors are small ($dF = \pm 7.3$ Jy, $d(\Delta v) = \pm 0.04$ $\mathrm{km\,s^{-1}}$ and $dv_{lsr} = \pm 0.02$ $\mathrm{km\,s^{-1}}$) and correspond to relative uncertainties of 5.5% in both flux density and linewidth. Thus, the statistical errors of the Gaussian line parameters of the strong 22 GHz water maser lines are in practice unsignificant for further analyses of the data.

However, since systematic errors in flux density (caused, e.g., by weather and/or gain problems) may play a role, we also consider how an estimated relative accuracy of 10% in flux density affects the linewidth and line velocity. For the median inside and outside maser the resulting realistic error in linewidth is 0.13 $\mathrm{km\,s^{-1}}$ and 0.11 $\mathrm{km\,s^{-1}}$, respectively. For both maser categories the error in line velocity is 0.06 $\mathrm{km\,s^{-1}}$, if the error in flux density is 10%.

It is noteworthy, that the variations seen in line velocity and linewidth during outbursts (e.g., Figs. 2 - 4) are not produced by the rms noise. They are also significantly larger than the realistic error estimates given above. Tables 2 - 4 show that the maximum variation in line velocity of these three maser outbursts is 0.20, 0.54, and 0.25 $\mathrm{km\,s^{-1}}$, respectively, which is 3.3, 9, and 4.2 times the realistic error in line velocity. For these three features the maximum variation in linewidth is 0.24, 0.66, and 0.77 $\mathrm{km\,s^{-1}}$, respectively, which is 1.8, 5.1, and 5.9 times the realistic error in linewidth. Generally, the linewidth is often at minimum at outburst maximum, but also random variations are quite common. No correlation exists between flux density and linewidth at outburst maxima (Liljeström and Gwinn 1999).

Most important, Liljeström and Gwinn (1999) found that the velocity dispersion derived from the variations in the single-dish line velocity during outbursts equals the velocity dispersion obtained with VLBI for maser spots within features. They suggest that the variations in Doppler velocity within maser features are caused by nonthermal velocity fluctuations of the medium and show that these line velocity variations together with the shock velocity and preshock density determine many important physical parameters of W49 N.

3.3 Correlated variability of maser features

During the 2.5 year monitoring period of W49 N, two major events per year occurred during which 12 - 14 maser features had their flux density maximum in the same relatively short time period (some 2 - 3 weeks). This is in accordance with earlier results (Sullivan 1973; Gammon 1976). By selecting only those events in the present study, which contained more than ten correlated outbursts, the proportion of coincidental outbursts (occurring by chance in the same time interval) was minimized. Table 5 presents the five major correlated events found in W49 N. It reveals that altogether 63 correlated outbursts took place during a total time period of 104 days. Because the number of reasonably well covered outbursts is in total 146, some 43% of all outbursts occurred in these correlated events during a time period corresponding to 11% of the whole monitoring period.

With help of Table 1 of Gwinn (1994b), 34 of the correlated outburst features could be identified and located on the VLBI map of W49 N (Fig. 2 of Gwinn et al. 1992). The fact that only 54% of the correlated outburst features could be identified is caused by the velocity gaps in the high-velocity data of Gwinn et al. (1992). In spite of this shortcoming, the following characteristics were found from the observed correlated outburst events.

Of the identified correlated outburst features, 62% took place in (and a few nearby) the most western subcluster of masers seen in Figure 2 of Gwinn et al. (1992). The offset of this subcluster (hereafter labeled A) from the expansion centre of the whole W49 N maser cluster (i.e., the origo of Fig. 2 of Gwinn et al. 1992) is about $-0.6''$ in rectascension. It is noteworthy, that this subcluster shows the largest blueshifted proper motions in Figure 2 of Gwinn et al. (1992). 29% of the identified correlated outburst features occurred in (and two nearby) the northeastern subcluster of masers in Figure 2 of Gwinn et al. (1992). This northeastern subcluster (hereafter labeled B) has an offset of $+0.6''$ in rectascension and is characterized by large redshifted proper motions.

Table 5 lists the identified subclusters in each correlated outburst event. It shows that outburst features in correlated events tend to belong to 1 - 2 subclusters characterized by high proper motions. Because 77% of all outbursts in W49 N were blueshifted, the blueshifted masers dominate also in the correlated outburst events. However, in the last event the majority of the outburst features are redshifted (9 redshifted and 3 blueshifted). Probably the 1 - 3 features with an opposite sign in their Doppler velocity (compared to the other features in the event) occur just by chance in the same time period.

In conclusion, masers in correlated outburst events are typically high-velocity features. On the VLBI map of Gwinn et al. (1992), the identified correlated features tended to belong to one blueshifted and one redshifted subcluster characterized by large proper motions. In addition, correlated outburst events tended to recur in the same maser subclusters. These characteristics suggest that correlated outbursts occur when traveling masers encounter local environmental changes (see Liljeström and Gwinn 1999).

Table 1: List of line velocities (in units of km s^{-1}) of 108 maser outburst features found in W49 N.

-233.5	-152.1	-75.1	-51.5	-10.1	28.3
-230.2	-144.6	-71.7	-47	-9.8	29.1
-277.7	-139.9	-66.4	-44.0	-9.77	34
-218.5	-138.5	-65.4	-42.3	-6.5	40.8
-210.4	-126.0	-64.8	-38.7	-5.5	41.2
-209.6	-124	-64.0	-37.4	-3.4	47.1
-209.0	-119.9	-63.2	-35	-0.9	47.8
-207.6	-113.5	-61.6	-32.6	3.3	53.7
-204.1	-107.2	-61.4	-30.4	5.8	73.1
-197.5	-105.8	-61.3	-27.7	8	98.8
-194.8	-105	-59.7	-26.0	10	106.6
-186.9	-94.3	-59.5	-24.4	12	107.8
-175.7	-90.8	-58.2	-22.5	13.3	118.8
-171.1	-88.2	-55.7	-20.3	14.9	124.1
-167.8	-79.1	-55.6	-19.0	16.5	141.0
-166.1	-78.9	-54.1	-16.5	16.9	153.2
-158.5	-77.3	-53	-15.6	20.2	156
-156.8	-77	-52.7	-14.8	22.0	177.7

References

Elitzur, M., Hollenbach, D. J., McKee, C. F. 1989, ApJ, 346, 983

Gammon, R. H. 1976, AA 50, 71

Genzel, R. and Downes, D. 1977, AASS, 30, 145

Genzel, R. et al. 1977, AA, 61, 117

Genzel, R. et al. 1981, ApJ, 247, 1039

Greenhill, L. J. et al. 1998, Nature, 396, 650

Gwinn, C. R. 1994a, ApJ, 429, 241

Gwinn, C. R. 1994b, ApJ, 429, 253

Gwinn, C. R., Moran, J. M., Reid, M. J. 1992, ApJ, 393, 149

Hollenbach, D. J. and McKee, C. F. 1979, ApJS, 41, 555

Hollenbach, D. J. and McKee, C. F. 1989, ApJ, 342, 306

Leppänen, K., Liljeström, T., Diamond, P. 1998, ApJ, 507, 909

Liljeström, T. and Gwinn, C. R. 1999, ApJ, 534, in press

Liljeström, T. et al. 1989, AASS, 79, 19

Little, L., White, G., Riley, P. 1977, MNRAS 180, 639

Malkamäki, L. 1983, Mitt. der Astron. Ges. 60, 466

Serabyn, E., Güsten, R., Schulz, A. 1993, ApJ, 413, 571

Sullivan III, W. T. 1971, ApJ, 166, 321

Sullivan III, W. T. 1973, ApJS, 25, 393

Ulich, B. L. and Haas, R. W. 1976, ApJS, 30, 247

Walker, R. C. et al. 1982, ApJ, 255, 128

White, G. J. and Macdonald, G. H. 1979, MNRAS, 188, 745

Table 2: Data file w49n-230.2.txt.
Observed parameters of the water maser feature at -230.2 $km\,s^{-1}$.

Julian date (JD-2440000)	v_{lsr} ($km\,s^{-1}$)	$\pm d(v_{lsr})$ ($km\,s^{-1}$)	Δv_{FWHM} ($km\,s^{-1}$)	$\pm d(\Delta v)$ ($km\,s^{-1}$)	Flux density (Jy)	$\pm dF$ (Jy)	rms noise (Jy)
5435.79	...	...	...	...	166	...	41.4
5441.77	-230.12	0.015	0.91	0.029	200	6.4	16.1
5445.67	-230.14	0.014	0.99	0.027	193	5.3	13.8
5449.71	-230.07	0.006	1.03	0.013	350	4.3	11.5
5458.77	-230.11	0.007	1.03	0.013	472	6.1	16.1
5461.68	-230.12	0.004	1.03	0.008	442	3.5	9.2
5468.40	-230.21	0.007	0.89	0.013	745	11.2	27.6
5472.74	-230.24	0.009	1.06	0.017	421	6.8	18.4
5479.68	-230.27	0.010	1.13	0.020	375	6.6	18.4
5483.74	-230.24	0.016	1.15	0.032	290	8.2	23.0
5489.39	-230.21	0.012	1.12	0.023	242	5.0	13.8

Table 3: Data file w49n-005.5.txt.
Observed parameters of the water maser feature at -5.5 $km\,s^{-1}$.

Julian date (JD-2440000)	v_{lsr} ($km\,s^{-1}$)	$\pm d(v_{lsr})$ ($km\,s^{-1}$)	Δv_{FWHM} ($km\,s^{-1}$)	$\pm d(\Delta v)$ ($km\,s^{-1}$)	Flux density (Jy)	$\pm dF$ (Jy)	rms noise (Jy)
4976.78	-5.81	0.003	1.29	0.006	1930	8.5	25.3
5009.74	-5.79	0.002	1.26	0.004	3170	11.0	32.2
5016.67	-5.84	0.001	1.23	0.003	3520	7.9	23.0
5018.64	-5.80	0.002	1.15	0.003	3750	10.7	29.9
5037.60	-5.68	0.001	1.04	0.002	5730	12.1	32.2
5038.64	-5.68	0.001	0.95	0.002	6100	9.9	25.3
5040.60	-5.68	0.001	0.94	0.002	6350	15.4	39.1
5058.56	-5.53	0.0006	0.80	0.001	9150	13.8	32.2
5062.55	-5.51	0.0006	0.82	0.001	8280	12.6	29.9
5065.60	-5.52	0.0007	0.84	0.001	8280	14.4	34.5
5078.49	-5.48	0.0006	0.86	0.001	6990	10.4	25.3
5097.49	-5.47	0.001	0.97	0.003	5800	17.0	43.7
5100.44	-5.40	0.001	0.96	0.002	5750	14.4	36.8
5102.44	-5.36	0.002	0.93	0.004	5860	22.8	57.5
5104.47	-5.30	0.001	0.93	0.003	5730	16.4	41.4
5121.38	-5.33	0.001	0.86	0.002	5040	14.2	34.5
5123.39	-5.36	0.002	0.87	0.004	4620	20.7	50.6
5142.30	-5.33	0.002	0.98	0.003	3680	12.4	32.2
5145.37	-5.38	0.001	0.93	0.003	3660	10.0	25.3
5148.37	-5.36	0.002	1.08	0.003	2880	9.3	25.3
5178.23	-5.43	0.004	1.16	0.008	2350	15.5	43.7
5183.21	-5.41	0.004	1.46	0.008	1900	10.9	34.5

Table 4: Data file w49n005.8.txt.
Observed parameters of the water maser feature at 5.8 km s^{-1}.

Julian date (JD-2440000)	v_{lsr} (km s^{-1})	$\pm$d(v_{lsr}) (km s^{-1})	Δv_{FWHM} (km s^{-1})	$\pm$d(Δv) (km s^{-1})	Flux density (Jy)	$\pm$dF (Jy)	rms noise (Jy)
4592.90	5.87	0.0005	1.41	0.0010	8920	6.7	20.7
4611.70	5.81	0.0007	1.34	0.0014	9780	9.9	29.9
4645.79	5.83	0.0001	1.01	0.0001	19700	2.6	6.9
4678.66	5.86	0.0003	0.99	0.0006	23200	13.2	34.5
4679.62	5.85	0.0001	0.99	0.0002	22500	4.4	11.5
4702.57	5.87	0.0003	0.91	0.0006	21900	13.8	34.5
4706.85	5.79	0.0003	0.95	0.0006	20700	12.6	32.2
4722.58	5.85	0.0002	1.18	0.0004	19000	5.7	16.1
4723.55	5.83	0.0001	1.17	0.0003	19700	5.7	16.1
4728.49	5.82	0.0002	1.20	0.0003	18700	4.8	13.8
4734.51	5.85	0.0002	1.24	0.0003	19400	4.7	13.8
4750.44	5.83	0.0002	1.26	0.0002	20900	6.3	18.4
4755.42	5.85	0.0001	1.14	0.0002	26400	5.8	16.1
4771.38	5.79	0.0001	0.99	0.0003	37300	10.6	27.6
4773.46	5.77	0.0002	0.98	0.0003	38000	13.3	34.5
4777.37	5.81	0.0001	0.96	0.0001	37000	4.5	11.5
4786.45	5.71	0.0001	0.96	0.0002	38000	8.1	20.7
4789.28	5.76	0.0001	0.96	0.0001	39100	5.4	13.8
4850.22	5.62	0.0002	1.13	0.0005	15900	6.6	18.4
4854.15	5.64	0.0002	1.13	0.0004	15300	5.8	16.1
4893.27	5.70	0.0003	1.40	0.0006	8000	3.7	11.5
4895.12	5.70	0.0001	1.63	0.0024	8260	12.4	41.4
4908.99	5.68	0.0004	1.68	0.0008	5730	2.7	9.2
4910.00	5.68	0.0005	1.58	0.0011	6030	4.2	13.8
4911.03	5.72	0.0005	1.61	0.0010	5500	3.5	11.5
4957.83	5.68	0.0021	1.58	0.0042	4190	17.5	57.5

Table 5: Major correlated outburst events found during the 2.5 year long monitoring period of W49 N.

Time period of the event	v_{lsr} of the features ($\mathrm{km\,s^{-1}}$)	Date of outburst maximum	Label of the maser subcluster[a]
17 - 29.4.1981	-175.70	17.04.1981	-
	-139.91	19.04.1981	A_2
	153.24	28.04.1981	B
	140.96	28.04.1981	B
	53.70	29.04.1981	-
	-22.49	29.04.1981	-
	-55.65	29.04.1981	A
	-63.20	29.04.1981	-
	-66.41	29.04.1981	-
	-79.14	29.04.1981	-
	-94.35	29.04.1981	-
	-119.93	29.04.1981	A_2
15.6 - 1.7.1981	-9.76	15.06.1981	A_1
	-37.41	15.06.1981	A
	-38.71	15.06.1981	A
	-79.13	17.06.1981	-
	10.39	17.06.1981	B
	21.99	17.06.1981	B_1
	-209.05	18.06.1981	-
	29.12	21.06.1981	B_1
	-77.23	21.06.1981	-
	-105.51	21.06.1981	-
	-107.18	21.06.1981	-
	-207.58	21.06.1981	-
	-194.80	01.07.1981	-
	5.76	01.07.1981	A_1
9 - 30.3.1982	12.25	09.03.1982	B
	-15.64	09.03.1982	A_1
	-44.14	09.03.1982	A
	-51.52	09.03.1982	A
	-210.35	09.03.1982	-
	8.23	12.03.1982	B
	-5.53	30.03.1982	A
	-22.13	30.03.1982	-
	-35.13	30.03.1982	A_1
	-53.70	30.03.1982	A

Table 5: — continued.

Time period of the event	v_{lsr} of the features ($\mathrm{km\,s^{-1}}$)	Date of outburst maximum	Label of the maser subcluster[a]
	-144.59	30.03.1982	-
	-171.14	30.03.1982	-
24.6 - 27.7.1982	16.91	24.06.1982	C
	-3.38	24.06.1982	A
	-18.96	24.06.1982	A
	-24.38	24.06.1982	-
	-77.27	27.06.1982	-
	-166.05	27.06.1982	A_2
	-204.10	27.06.1982	-
	-0.91	27.07.1982	C_1
	-16.46	27.07.1982	A
	-46.71	27.07.1982	A
	-78.88	27.07.1982	-
	-156.73	27.07.1982	A_2
	-158.49	27.07.1982	A_2
21.3 - 10.4.1983	5.32	21.03.1983	A_1
	13.30	21.03.1983	B
	20.23	21.03.1983	B
	28.33	21.03.1983	-
	33.77	21.03.1983	-
	98.76	21.03.1983	-
	107.86	07.04.1983	-
	-20.27	07.04.1983	-
	-59.55	07.04.1983	-
	41.15	09.04.1983	-
	-1.20	10.04.1983	C_1
	34.57	10.04.1983	-

[a] The subclusters have been identified using Table 1 of Gwinn (1994b). The labeled subclusters have the following approximate offsets in right ascension and declination (in units of arcseconds) from the origo of Fig. 2 of Gwinn et al. (1992):
A(-0.6, 0.2); A_1(-0.6, -0.2); A_2(-0.9, 0.2);
B(0.6, 0.5); B_1(0.6, 0.3);
C(0.2, 0.4); C_1(0.002, 0.0004).

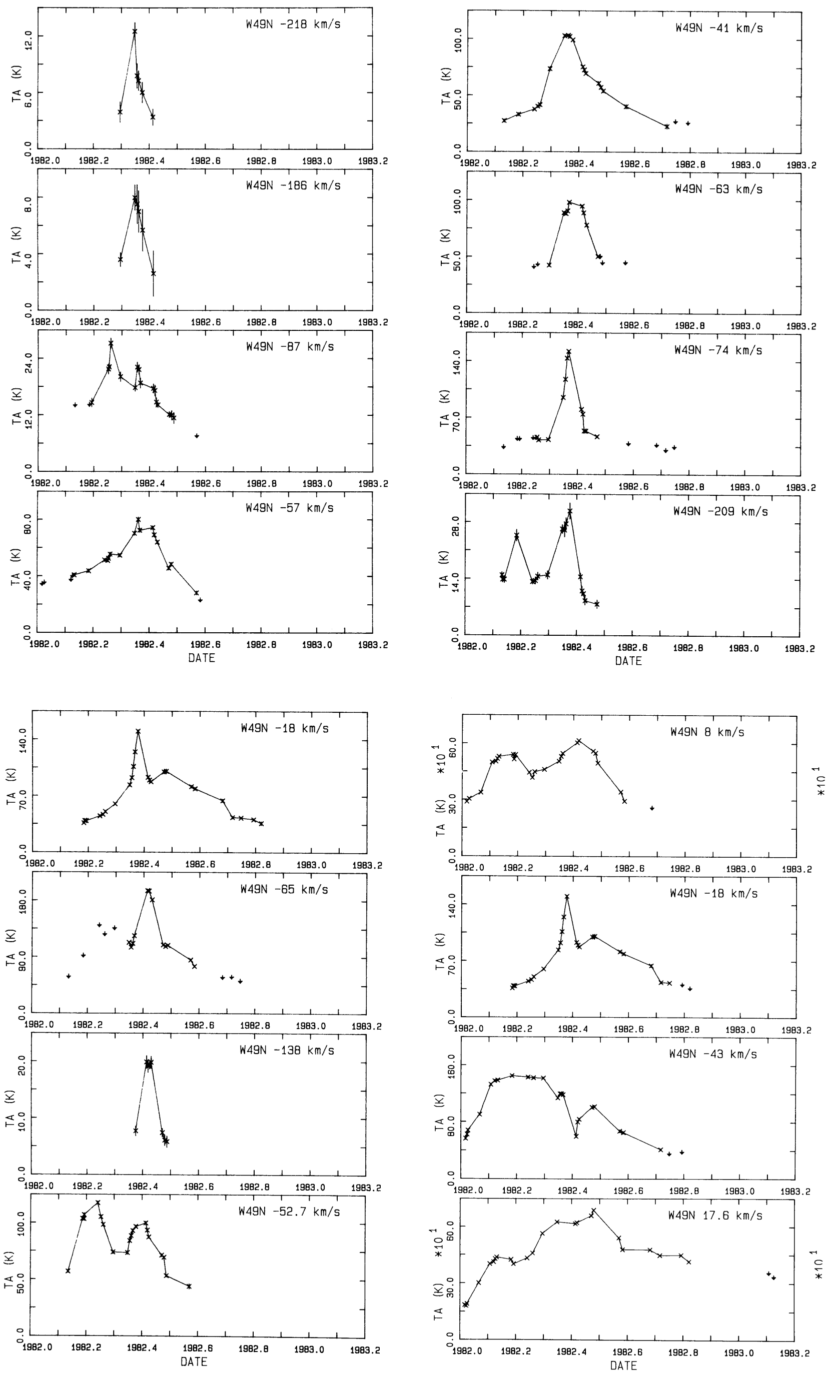

Figure 1: Water maser outbursts of W49 N ordered as function of time. One figure file (w49nfig1g.ps) of 11 is shown as an example. 1 K of the antenna temperature, T_A, corresponds to 23 Jy.

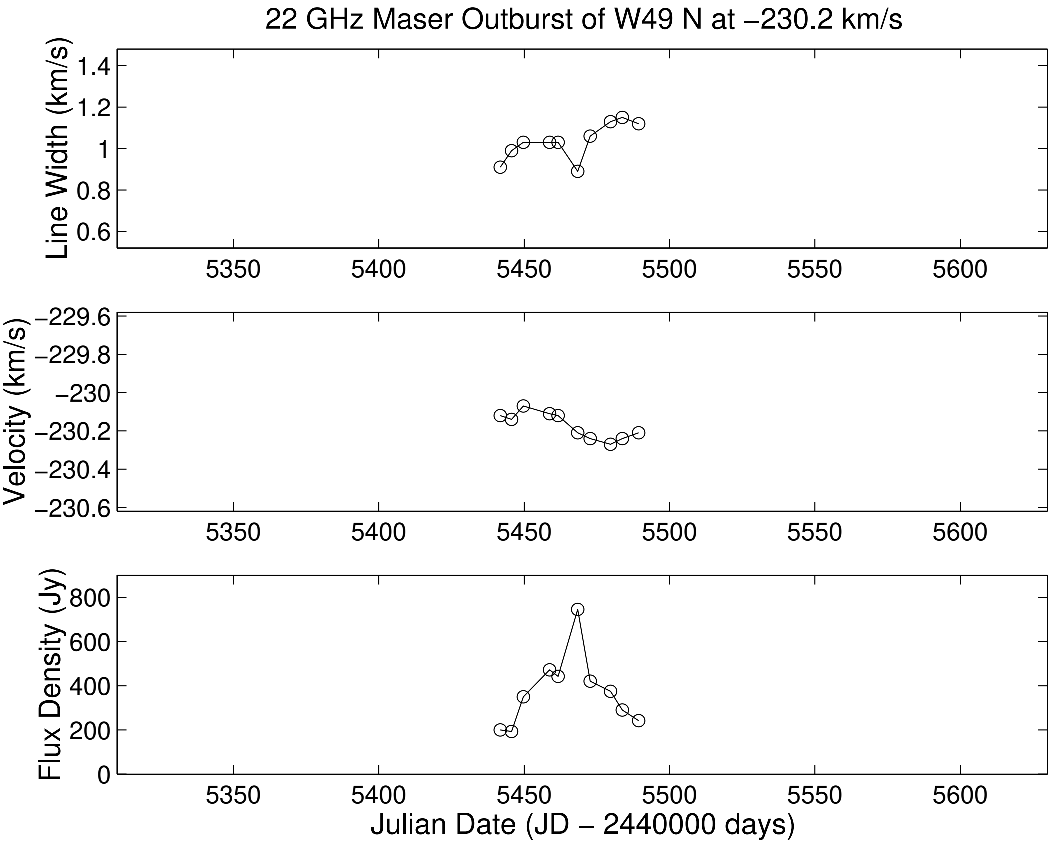

Figure 2: Graphical presentation of Table 2.

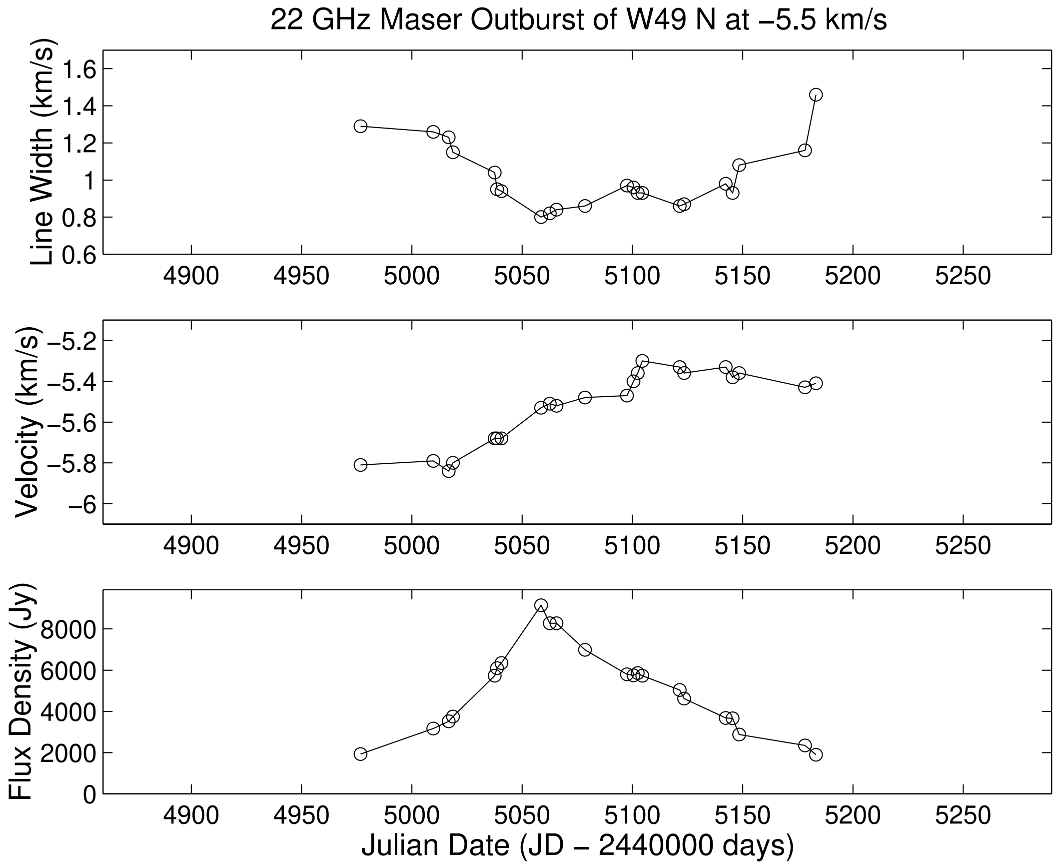

Figure 3: Graphical presentation of Table 3.

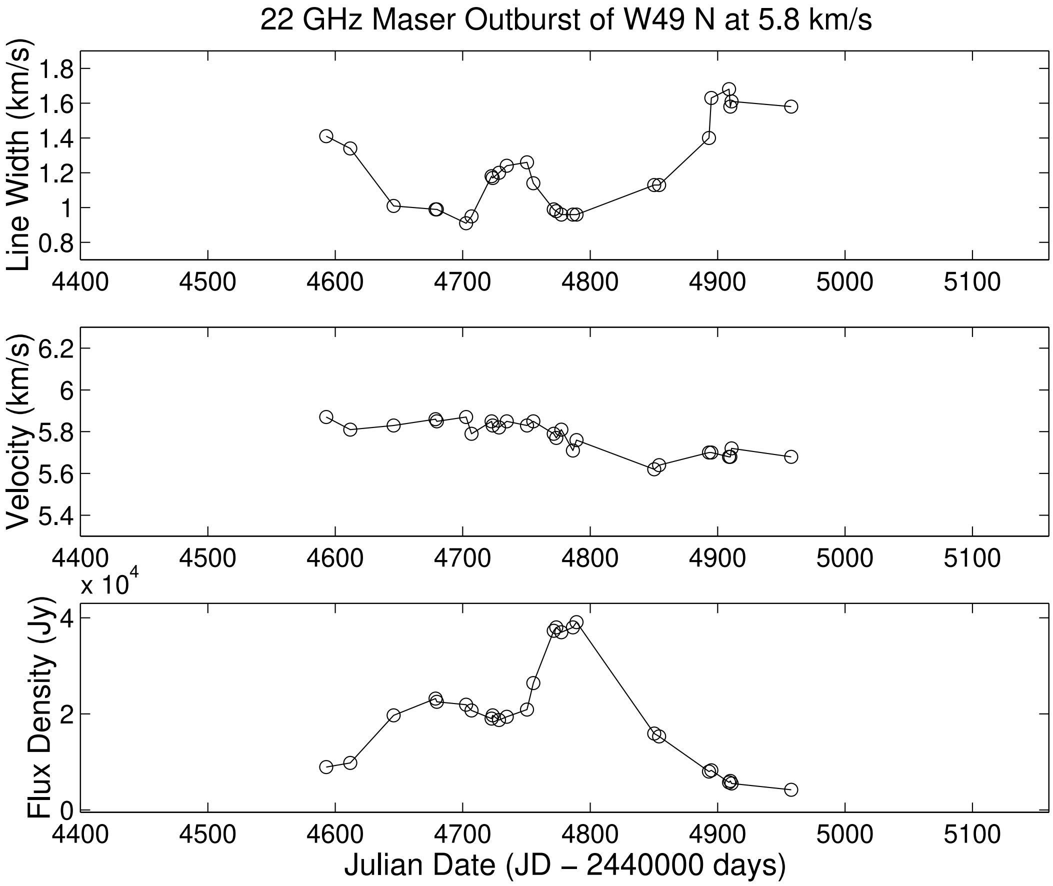

Figure 4: Graphical presentation of Table 4.